Supplementary Information (SI) for New Journal of Chemistry.
This journal is © The Royal Society of Chemistry 20xx

Supplementary Information

Lanthanum-modified Hydroxyapatite-Supported Cobalt for Highly Selective Synthesis of Primary Amines via Ethylene Glycol Amination

*Bin Zhou, Yingjie Guan, Xin Gao, Jisheng Yu, Jinglong Pu, Huilin Chen, Xue Wang, Dongxue Yi, Yuhao Song, Gaoyu Li, Rui Zhang, * and Xuedong Zhu **

State Key Laboratory of Chemical Engineering and Low-Carbon Technology, Engineering Research Center of Large-Scale Reactor Engineering and Technology (Ministry of Education), East China University of Science and Technology, Shanghai, 200237, PR China

Corresponding author

Xuedong Zhu* - E-mail: xdzhu@ecust.edu.cn

Rui Zhang* - E-mail: r.zhang@ecust.edu.cn;

Catalyst Characterization Procedures: X-ray diffraction (XRD) measurements were conducted using a RIGAKU diffractometer with Cu Kα radiation, operated at 40 kV and 100 mA. Both low-angle and wide-angle diffraction patterns of the powder were recorded in the 2θ range of 25°-35° and 10°-80°, respectively.

Specific surface area and pore structure measurements were obtained through N_2 adsorption/desorption using a BSD-660 fully automatic high-throughput specific surface area and pore size analyzer at -196°C, after the samples were degassed at 300°C under vacuum. The specific surface area was calculated using the Brunauer-Emmett-Teller (BET) method, while the pore properties were determined using the Barrett-Joyner-Halenda (BJH) method.

Inductively Coupled Plasma Optical Emission Spectroscopy (ICP-OES) was conducted to determine the actual Co loading and La content using an Agilent 5800 ICP-OES (USA).

Thermogravimetric (TG) analysis was conducted using a TA Discovery TGA 550 (USA) instrument under an N_2 atmosphere. The test temperature range was 50~800°C with a heating rate of 10°C/min.

Transmission electron microscopy (TEM) imaging was conducted using a JEM-2100F transmission electron microscope operating at 200 kV. Scanning transmission electron microscopy coupled with energy-dispersive X-ray spectroscopy (STEM-EDS) was

performed on a ZEISS Sigma 500 Field Emission Scanning Electron Microscope, equipped with an Oxford Xplore Energy Dispersive X-ray Spectrometry (EDS) detector.

X-ray photoelectron spectroscopy (XPS) measurements were performed using a Thermo Scientific K-Alpha spectrometer. The binding energies were calibrated using the C 1s peak, set at 284.8 eV.

Temperature-programmed reduction by hydrogen (H_2-TPR) was performed using a Micromeritics Chemisorb 2720 analyzer. During the experiment, the oxides were heated in H_2 (10 vol%)/Ar gas flow from 50 to 700^{o}C at a ramp rate of 10^{o}C/min, with profiles recorded by a thermal conductivity detector (TCD). Temperature-programmed desorption (TPD) was carried out on the same apparatus as the TPR.

In-situ DRIFTS measurements were performed using a Nicolet iS50 spectrometer. Prior to adsorption, the samples were reduced at 450^{o}C for 2 hours under H_2. After reduction, Ar was introduced, and the temperature was gradually lowered to 240^{o}C, 220^{o}C, 200^{o}C, 180^{o}C, and 160^{o}C, respectively, with the background spectrum recorded at each temperature. EG vapor was then introduced at 80^{o}C, and the spectrum was recorded until the signal stabilized. The temperature was subsequently increased to the next set point, and the sampling process was repeated.

Materials: Ammonium dihydrogen phosphate ($(NH_4)_2HPO_4$,≥99.0%), Calcium nitrate tetrahydrate ($Ca(NO_3)_2{\cdot}_4H_2O$, ≥99.0%), Ethylene glycol (EG, ≥99.5%), Tetrahydrofuran (THF, ≥99.5%), Tetradecane ($C_{14}H_{30}$, ≥99.0%), Hexahydrate lanthanum nitrate

($La(NO_3)_3 \cdot 6H_2O$, ≥99.0%), Iron(III) nitrate nonahydrate ($Fe(NO_3)_3 \cdot 9H_2O$, ≥99.0%), Hexahydrate nickel nitrate ($Ni(NO_3)_2 \cdot 6H_2O$, ≥99.0%), Zinc nitrate hexahydrate ($Zn(NO_3)_2 \cdot 6H_2O$, ≥99.0%), Manganese nitrate tetrahydrate ($Mn(NO_3)_2 \cdot 4H_2O$, ≥99.0) and Strontium nitrate ($Sr(NO_3)_2$, ≥99.5%) were all purchased from Sinopharm Chemical Reagent Co., Ltd. Ammonia ($NH_3 \cdot H_2O$, 25%-28%) and Copper nitrate ($Cu(NO_3)_2$, ≥99.0%) were purchased from Macklin.

HAP preparation: 56 mL of 0.6 M $Ca(NO_3)_2 \cdot 4H_2O$ and 50 mL of 0.4 M $(NH_4)_2HPO_4$ solution were each adjusted to pH 10.5 using ammonia. The $Ca(NO_3)_2$ solution was then slowly added to the $(NH_4)_2HPO_4$ solution under stirring, while ammonia was used to maintain the pH at 10.5 until no further precipitation occurred. The suspension was stirred at 80°C for 3 hours. The resulting solid was aged at room temperature for 24 hours, washed three times with deionized water, dried overnight at 110°C, calcined at 600°C for 2 hours, and then ground to obtain HAP powder (Scheme S1).

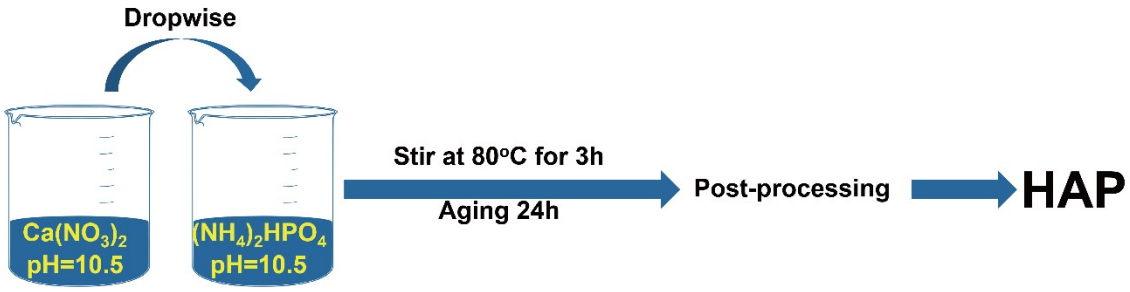

Scheme S1. HAP preparation process

Doped HAP preparation: Using $M(NO_3)_x \cdot yH_2O$ (M = Sr, Ni, Co, Zn, La) as the dopant metal source, a 50 mL solution of 0.4 M $(NH_4)_2HPO_4$ was prepared in advance. The required amount of $M(NO_3)_x \cdot yH_2O$ and $Ca(NO_3)_2 \cdot 4H_2O$ were dissolved in deionized water, maintaining the molar ratio of (Ca+M)/P = 1.67 and M/Ca = 0.1. Both solutions were adjusted to pH 10.5 with ammonia. Under stirring, the (Ca+M) mixture solution was slowly added to the $(NH_4)_2HPO_4$ solution, with ammonia used to maintain the pH at 10.5 until no further precipitation occurred. The suspension was stirred at 80°C for 3 hours. The resulting solid was aged at room temperature for 24 hours, washed three times with deionized water, dried overnight at 110°C, calcined at 600°C for 2 hours, and ground to obtain M-doped HAP powder.

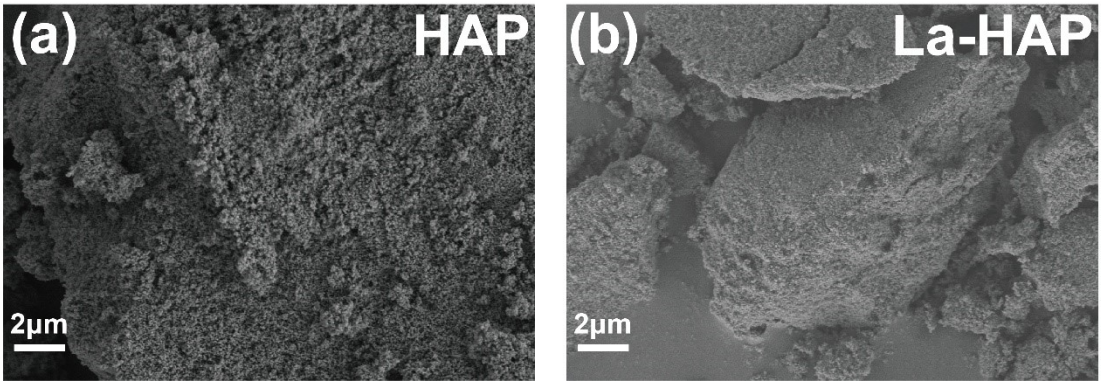

Figure S1. SEM images of (a) HAP and (b) La-HAP.

The SEM image of HAP (Figure S1) shows that it exhibits amorphous characteristics, consistent with previous reports[1]. After the addition of La, the morphology of La-HAP did not change significantly and still appeared as large, irregular shapes. However, compared

to HAP, the surface of La-HAP was smoother, indicating lower crystallinity[2], which is consistent with the XRD results. These observations confirm that La incorporation does not alter the overall morphology of HAP but reduces its crystallinity.

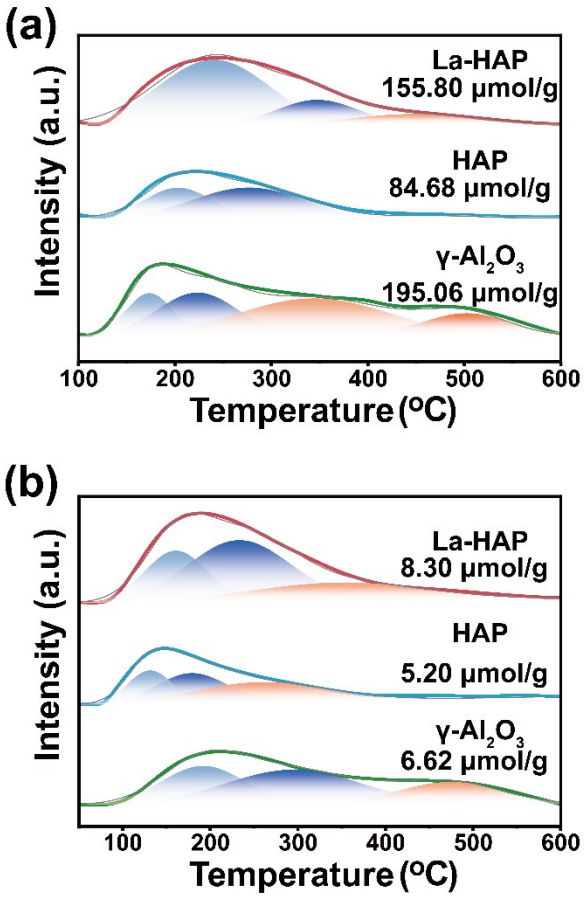

Figure S2. (a) NH_3-TPD and (b) CO_2-TPD images of La-HAP, HAP and γ-Al_2O_3

Figure S2 shows the NH_3-TPD (Figure S2a) and CO_2-TPD (Figure S2b) profiles of La-HAP, HAP, and γ-Al_2O_3. It can be observed that after La doping, both the acid and base contents of La-HAP increased compared to HAP, rising from 84.68 μmol/g and 5.20 μmol/g to 155.8 μmol/g and 8.3 μmol/g, respectively. This pattern aligns with the TPD

behavior observed after Co loading. Prior to Co loading, γ-Al_2O_3 exhibited acid and base amounts of 195.06 μmol/g and 6.62 μmol/g, respectively.

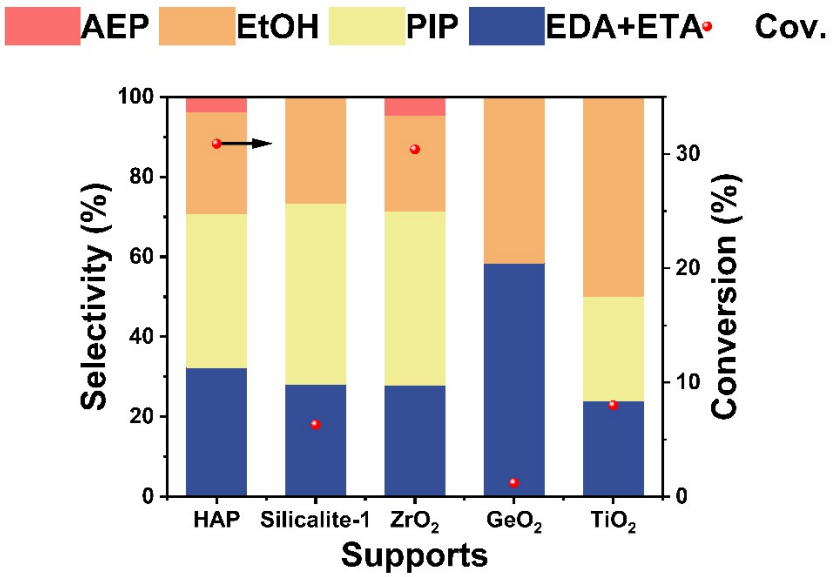

Figure S3. Catalytic effects of Co loaded on different supports. Reaction conditions: T = 453 K; catalyst mass = 0.25 g; EG mass = 0.5 g; P_{NH_3} = 0.6MPa; P_{H_2} = 1.5MPa; Reaction time = 8 h

Table S1. Catalytic effects of different metals

Metal	Conversion (%)	Selectivity (%)				
		ETA	EDA	EtOH	PIP	AEP
Co	30.9	9.2	24.4	13.1	47.7	5.6
Ni	10	11.1	30.8	26.2	29.0	2.9
Cu	0	0	0	0	0	0
Fe	0	0	0	0	0	0
Mn	0	0	0	0	0	0

[a] Reaction conditions: T = 453 K; catalyst mass = 0.25 g; EG mass = 0.5 g; P_{NH_3} = 0.6MPa; P_{H_2} = 1.5MPa; Reaction time = 8 h

We first conducted a preliminary screening of different supports and metals, with the results summarized in Figure S3 and Table S1. The Co/HAP composite, obtained by combining Co with HAP, serves as an active catalyst for the amination of EG, achieving 30.9% EG conversion with 32.4% selectivity to the primary amine under the given conditions.

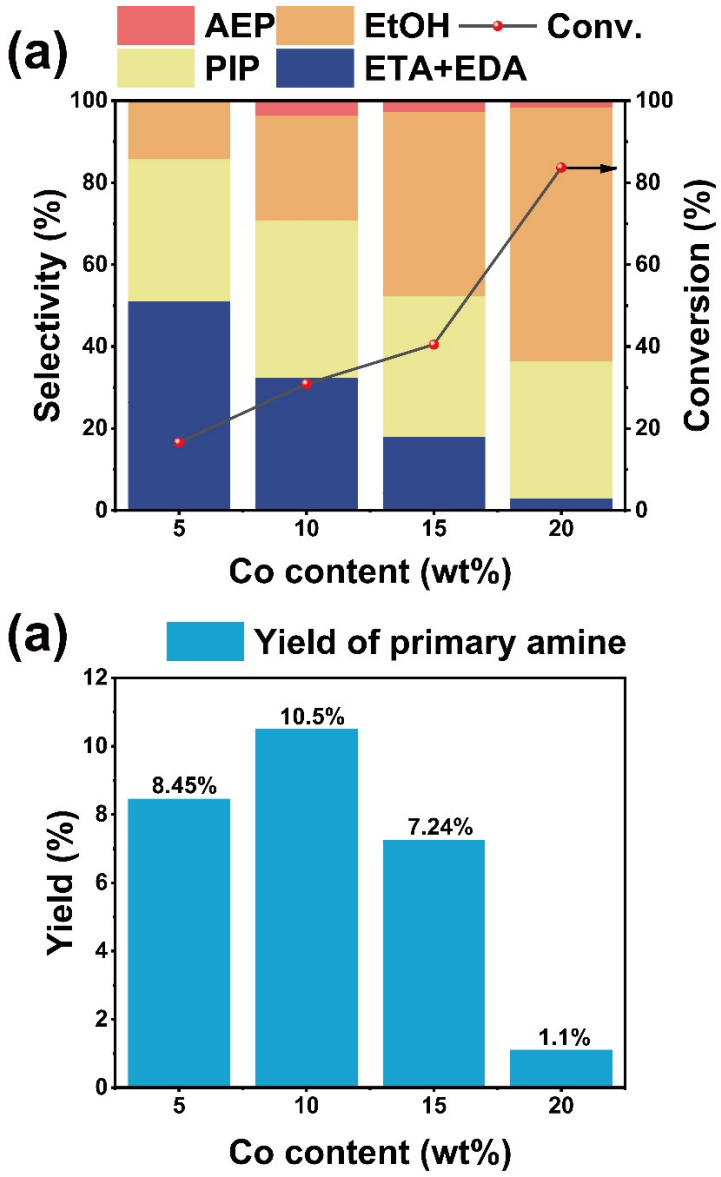

Figure S4. Catalytic performance of Co/HAP with different Co loadings: (a) product distribution and (b) primary amine yield. Reaction conditions: T = 453 K; catalyst mass = 0.25 g; EG mass = 0.5 g; P_{NH_3} = 0.6MPa; P_{H_2} = 1.5MPa; Reaction time = 8 h

Figure S4 illustrates the catalytic performance of Co/HAP catalysts with varying Co loadings on EG amination. As the Co loading increases, the catalytic activity improves, while the selectivity for primary amines decreases progressively (Figure S4a). For the 20

wt% Co/HAP catalyst, the ethylene glycol conversion rate reaches 83.7%, but the primary amine selectivity is only 2.9%. Considering the overall yield (Figure S4b), 10 wt% Co loading was identified as the optimal loading. Further, the effects of various doped metals are presented in Figure S5. When La is used as the dopant, Co/La-HAP exhibits exceptional primary amine selectivity, reaching 65.5%.

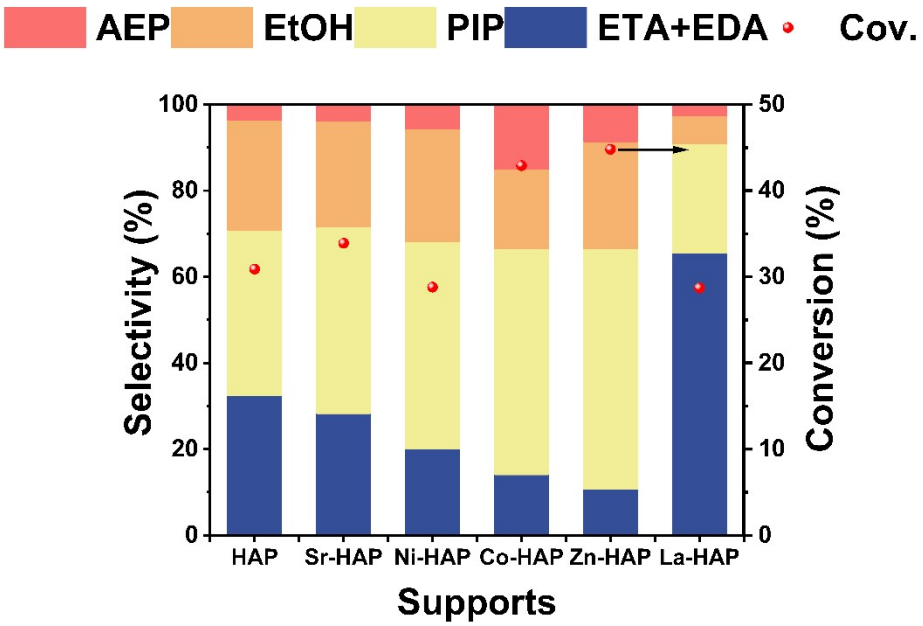

Figure S5. Screening of modified metals. Reaction conditions: T = 453 K; catalyst mass = 0.25 g; EG mass = 0.5 g; P_{NH_3} = 0.6MPa; P_{H_2} = 1.5MPa; Reaction time = 8 h

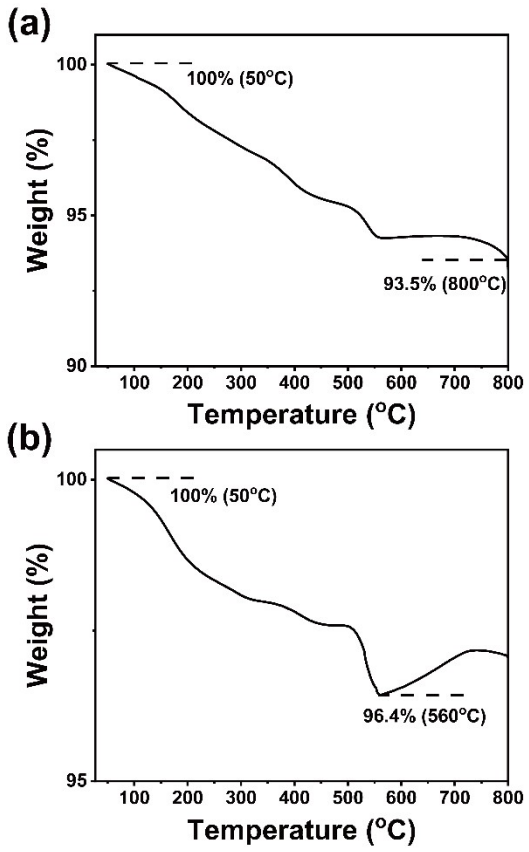

Figure S6. TG curves of (a) Co/HAP and (b) Co/La-HAP after cyclic reaction

Figure S6 displays the TG curves of Co/HAP (Figure S6a) and Co/La-HAP (Figure S6b) after cyclic reaction. Both catalysts exhibit slight mass loss with increasing temperature, indicating the formation of minor carbonaceous species on both catalysts following cyclic reaction. Co/HAP exhibited its maximum mass loss at 800°C, losing approximately 6.5%, while Co/La-HAP reached its maximum mass loss at 560°C, losing about 3.6%.

Table S2. Co content in Co/HAP and Co/La-HAP after cyclic reaction

Samples	Co Content (wt%)[a]
Co/HAP	7.7
Co/La-HAP	7.5

[a] The values were measured by ICP-OES analysis.

Following the cyclic reaction, the Co content on both catalysts exhibited a significant decrease. The mass fraction of Co on Co/HAP and Co/La-HAP decreased from 9.2 to 7.7 and 7.5, respectively. This reduction may be attributed to the desorption of Co species due to prolonged stirring of the catalysts in the batch reactor.

In summary, based on thermogravimetric analysis and elemental analysis of the spent catalysts, we conclude that coking and the desorption of Co species from the catalyst surface are the primary causes of catalyst deactivation in the batch reactor.

Reference

1. C. R. Ho, V. Defalque, S. Zheng and A. T. Bell, *ACS Catalysis*, 2019, **9**, 2931-2939.
2. S. Hibino, T. Todo, T. Ishimoto, O. Gokcekaya, Y. Koizumi, K. Igashira and T. Nakano, *Crystals*, 2021, **11**.